JOURNAL OF CATALYSIS 57, 406–416 (1979)

Hydrogenation of Surface Carbon on Alumina-Supported Nickel[1]

J. G. McCarty and H. Wise

Solid-State Catalysis Laboratory, SRI International, Menlo Park, California 94025

Received March 27, 1978; revised November 29, 1978

Four types of carbon were observed to form on an alumina-supported nickel methanation catalyst on exposure to carbon monoxide at 550 ± 50 K. In order of their reactivity toward hydrogen the carbon species may be classified as: chemisorbed carbon atoms (α), bulk nickel carbide, amorphous carbon (β), and crystalline elemental carbon. The α-phase and the initial monolayers of Ni_3C are much more reactive than the elemental forms as measured by temperature-programmed surface reaction in 100 kPa H_2. At 550 K the α- and β-carbon species formed by CO exposure populate the surface at a ratio of about 2:1. Both phases are relatively stable on heating to 600 K in a He atmosphere. At higher temperatures, slow conversion of α- and β-carbon to graphite was observed. Hydrogenation of the α state at 550 K leads to methane at a sufficiently fast rate to make it a likely intermediate in nickel-catalyzed methane synthesis from hydrogen and carbon monoxide.

INTRODUCTION

Despite considerable research effort over the past 50 years, the mechanism of hydrogenation of the oxides of carbon catalyzed by transition metals remains elusive (*1*, *2*). It needs to be demonstrated whether catalytic methanation and Fischer–Tropsch synthesis on such catalysts as Ni, Fe, Co, and Ru require breakage of the C-to-O bond as an elementary step preceding hydrogen addition.

Direct observation of carbon monoxide dissociation on clean iron (*4*) and nickel (*5*) surfaces has stimulated renewed interest in the mechanism of methanation. Recent studies (*6*, *7*) have shown that carbon adspecies are intermediates in methanation, as postulated earlier for Fischer–Tropsch synthesis (*3*, *8*). Thus, carbon deposited on supported nickel catalysts (*6*) and nickel films (*7*) by dissociative chemisorption of carbon monoxide at elevated temperatures readily produces methane upon subsequent exposure to hydrogen.

In the present work, the methanation of carbon deposited on an alumina-supported nickel methanation catalyst was studied using temperature-programming techniques. Both the chemical nature of surface carbon and the kinetics of reaction with hydrogen were determined using temperature-programmed surface reaction (TPSR).

EXPERIMENTAL DETAILS

Catalyst. In our measurements we used an alumina-supported Ni catalyst.[2] The catalyst, originally in the form of $\frac{1}{8}$-in.

[1] Support of this research by the American Gas Association is gratefully acknowledged.

[2] The catalyst, Girdler G-65, contained 25 wt% nickel, 8 wt% "alkali" (primary CaO), and 4 wt% carbon as graphite. This carbon was found to be relatively inert, as discussed in greater detail in another section of this report.

0021-9517/79/060406-11$02.00/0

extruded pellets, was crushed, ground, and screened to 75 ± 12-μm particles (170/250 mesh). This catalyst was particularly suited to our studies because of its high nickel surface area per unit weight and its resistance to sintering at temperature up to 800 K. Pretreatment of the catalyst included reduction at 725 ± 10 K in 1 atmosphere of hydrogen for 15 to 16 hr at a space velocity of 5×10^4 hr^{-1}.

The specific metal surface area of the catalyst after reduction in H_2 was found to be 23 ± 1 m^2/g of nickel, as determined by carbon monoxide adsorption at 300 K using a pulsed flow technique (described below). The saturation coverage was taken to be 1.0×10^{15} molecules of CO/cm^2 metal.

Apparatus. The TPSR experiments were conducted in a small, vertically mounted quartz microreactor containing a porous glass frit onto which approximately 15 to 30 mg of powdered catalyst was placed. Carrier gases, helium or hydrogen, passed through the catalyst bed. Heat was indirectly supplied by a resistively heated Nichrome wire surrounding the reactor. A programmable dc voltage power supply was used to heat the reactor from 300 to 800 K at nearly linear rates variable from 0.2 to 1.5 $K \cdot s^{-1}$. The temperature was measured with a 0.003-in. Chromel-Alumel thermocouple which extended into and made thermal contact with the catalyst bed. The response of the thermocouple to a change in heat input was approximately 2 s.

Gases. Adsorbant or reactant gases were admitted to the catalyst by injecting 0.55-cm^3 aliquots (NTP) of the gas into the purified helium or hydrogen carrier upstream of the catalyst bed. The helium carrier stream was purified by sequential passage through a bed of copper foil heated to 525 K followed by a liquid nitrogen-cooled molecular-sieve trap. The hydrogen carrier stream was purified by diffusion through a palladium thimble. The residual amount of oxygen in the He or H_2 carrier stream was routinely measured with the mass spectrometer and found to be typically less than 0.5 ppm. The other gases used in this study—research grade 2.85 vol% carbon monoxide in helium, 1.21 vol% ethylene in helium, 3.19 vol% methane in helium, 3.19 vol% carbon dioxide in helium, and 1.03 vol% hydrogen in helium—were not subjected to further purification. An eight-port (Loenco) gas chromatograph switching valve, with double Viton O-ring seals between ports, was used to inject these gases into the carrier stream.

Analysis. The gas composition downstream of the reactor was monitored with a quadruple mass spectrometer (EAI), which analyzed a portion of the effluent gas stream admitted into the vacuum system through the variable-leak valve of a vacuum pressure controller. Selected components of the effluent gas stream (up to a limit of eight) could be simultaneously analyzed using an automatic peak selector to drive the mass spectrometer.

The mass spectrometer system was calibrated by sampling a dilute reference gas of known composition (e.g., 3.19 vol% CH_4/He, 3.19 vol% CO_2/He); during calibration the reactor was bypassed using a six-port O-ring sealed GC valve. The mass spectrometer was also calibrated with aliquots of the reference gas injected into the carrier stream.

Carbon deposition. Carbon was deposited on a freshly reduced catalyst sample by exposure either to CO or ethylene at elevated temperatures. After hydrogen reduction the catalyst was flushed with helium for several minutes at a temperature above 600 K. Subsequent pulses of the carbon-bearing gas (0.65 μmol CO/pulse or 22 μmol C_2H_4/pulse) were injected into a helium carrier (100 kPa), with the bed held at the desired temperature in the range from 500 to 625 K. The concen-

trations of CO and CO_2 in the reactor effluent were monitored simultaneously during exposure to CO, from which the net carbon and oxygen uptake could be determined. C_2H_4 was especially suited for producing bulk carbon and bulk carbide since the carbon deposition rate during CO exposure was found to slow considerably with increasing carbon surface coverage. During injection of C_2H_4 the formation of H_2 and CH_4 was observed but not quantitatively analyzed.

The time period for carbon deposition with CO varied from 200 to 500 s depending upon the number of CO pulses used. For subsequent TPSR measurements, the catalyst bed was cooled to room temperature and the carrier gas switched to H_2 after the CO or CO_2 concentration approached a stable baseline value, which required about 100 s. However, in a few experiments designed to measure the rate of conversion of active surface carbon to other carbon configurations, the catalyst was left in the helium carrier for another 420 s at the desired temperature after exposure to CO pulses.

Temperature programmed surface reaction. Following carbon deposition the catalyst bed was cooled in flowing helium to room temperature and the carrier gas switched to hydrogen. The catalyst bed temperature was then increased at a nearly linear rate variable from 0.2 to 2.0 K/s from 300 to 775 K while monitoring the effluent gas composition. The 15 AMU ion fragment (CH_3^+) was used to measure the methane concentration. The concentration of higher molecular weight hydrocarbons (to C_5) was found insignificantly small relative to CH_4, e.g., C_2 hydrocarbons were $<1\%$ of the CH_4 yield.

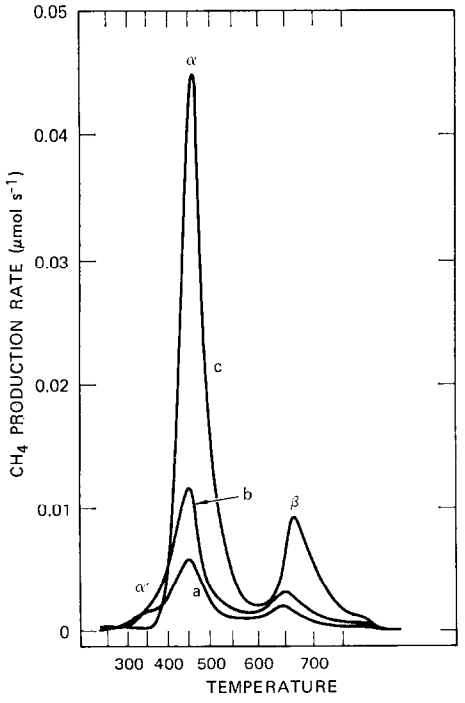

FIG. 1. TPSR with H_2 following carbon deposition by exposure of Ni/Al_2O_3 to CO at 550 ± 3 K. Relative carbon deposit (a) 0.48, (b) 1.19, (c) 3.14 (see text). Heating rate = 1.00 ± 0.15 K·s^{-1}.

RESULTS

Reactivity of Surface Carbon Deposited by Dissociative Adsorption of Carbon Monoxide

High surface coverage with carbon rather than CO was desired for our studies. Such a condition was attained by exposing the small catalyst sample to a number of consecutive CO pulses in a He stream at 500 to 625 K. Initially only small amounts of CO and CO_2 were detected in the effluent stream; however, after exposure to several CO pulses the evolution of CO_2 and CO were found to increase, indicative of (1) the removal of oxygen adatoms by reaction with CO, and (2) the progressive occupation of surface sites by carbon to the point where in terms of a mass balance the chemisorbed CO represented a small part of the surface population. The surface carbon coverage is expressed in terms of an arbitrary monolayer parameter, with one monolayer defined as the amount of CO adsorbed at 296 K and 5 Pa. Following the deposition of carbon, the catalyst was

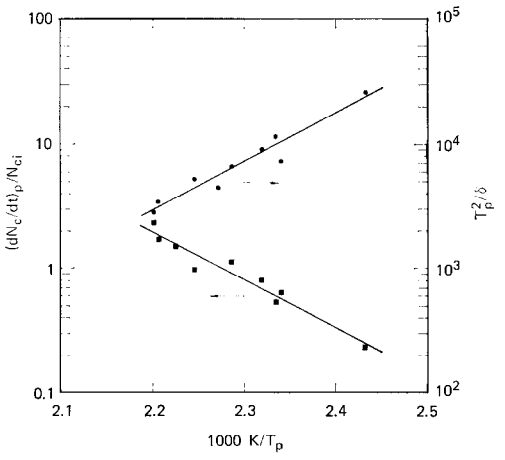

FIG. 2. Kinetic analysis of TPSR for reaction between surface carbon (α-state) and gaseous hydrogen catalyzed by Ni/Al_2O_3 (25 wt%).

rapidly cooled to 300 K in helium stream (~60 s). Then the carrier gas was switched from helium to hydrogen (100 kPa) and temperature programming was initiated.

Figure 1 shows a series of TPSR curves for reaction of the carbon deposit with H_2 as a function of carbon coverage. The reaction rate was calculated from the carrier gas flow rate and the time-dependent CH_4 concentration, as measured with the mass spectrometer, and plotted against the time-dependent catalyst temperature, as monitored by the thermocouple.

Two distinct carbon species are observed based on their reactivity toward H_2: (1) a highly reactive form, which we shall designate α-carbon, with a peak temperature, $T_p = 470 \pm 20$ K, that is the temperature of maximum CH_4 evolution rate at the specified heating rate, and (2) a less reactive form, designated β-carbon, with $T_p = 680 \pm 30$ K. It is to be noted that for both states the T_p values, the TPSR peak shapes, and the α to β coverage ratio did not vary significantly with initial total carbon coverage. In addition, at low coverage a very reactive α' state was detectable (Fig. 1) with CH_4 formation observable at 325 K. In fact, some methane was produced at temperatures as low as 300 K.

In analogy to temperature-programmed desorption (*9*) (TPD), the apparent activation energy, E, and preexponential coefficient, A, can be evaluated (*10*) from TPSR measurements by means of a graphical procedure using semilogarithmic plots of $(dN_c/dt)_p/N_{ci}$ versus $1/T_p$, and T_p^2/δ versus $1/T_p$. In this case the function $(dN_c/dt)_p$ is the maximum carbon removal (or methane production rate), N_{ci} is the total α-carbon initially present, and δ is the heating rate. The following assumptions are made in the analysis: (1) the reaction is irreversible and goes to completion without interference from competing or subsequent reactions (2) the rate is a single valued function of coverage and temperature, and (3) the temperature dependence of the rate does not vary with coverage and can be expressed in Arrhenius form applied to TPSR. The analysis also requires constant linear heating rate, δ, and constant H_2 pressure. The first-order frequency factor presumes that the rate is directly proportional to carbon coverage in a given state. However, analysis of the slopes of the semilogarithmic plots, which are proportional to the activation energy, are not affected by the nature of the coverage dependence.

The kinetic analysis of the TPSR experiments for the α-carbon state is shown in Fig. 2. Despite variation in initial surface coverage (from 0.5 to 1.5) and some nonlinearity in the heating rate, the values for the activation energy obtained by least squares analysis are in remarkably good agreement, $E = 71.3 \pm 18.1$ and 71.1 ± 19.6 kJ·mol^{-1}, for $(dN_c/dt)_p$ or T_p^2/σ versus $1/T_p$, respectively. The calculated frequency factors are found to be: $A = 3.4 \times 10^6$ s^{-1} and 2.5×10^6 s^{-1}, respectively. The same procedure was applied to the evaluation of the kinetic parameters for β-carbon.

An increase in the temperature of carbon deposition by dissociative chemisorption of CO had a minor effect on the TPSR spectra. In general, the distribution of carbon coverage in the α and β states changed from $\alpha/\beta \cong 2$ at $T \leq 550$ K to $\alpha/\beta \cong 1$ at $T = 600$ K.

Surface Carbon from Ethylene Decomposition

Surface carbon formed by exposure of the Ni/Al_2O_3 catalyst to pulses of ethylene at 575 K was subjected to a series of TPSR experiments in hydrogen.[3] The results (Fig. 3) show a number of carbon binding states with increasing coverage, labeled as α ($T_p = 495$ K), β ($T_p = 700$ K), and γ ($T_p = 550$ K). We have identified the carbon state at 495 K as α and the one at 550 K as γ, although the two states show considerable overlap.

An increase in carbon coverage (Fig. 3) caused a relatively large increase in the size of the β and γ states. For curve d in Fig. 3 the total amount of carbon converted to CH_4 by TPSR in H_2 amounts to 11 times the saturation CO uptake measured at 300 K on the fresh sample. This result suggests that the γ state represents bulk carbide, most likely Ni_3C. Also the high population of the β state, also of magnitude greater than monolayer coverage, indicates the presence of another bulk phase, presumably in this case amorphous carbon. Both the β and γ states shifted to higher temperature with increasing carbon deposition as would be expected for bulk phases.

Transformation of α- to β-Surface Carbon

The thermal stability of α-carbon over the temperature range from 600 to 750 K was determined in a series of experiments, in which carbon was first deposited on the Ni/Al_2O_3 catalyst at 560 ± 3 K by

[3] During dosing with C_2H_4, the formation of H_2 and CH_4 was detectable.

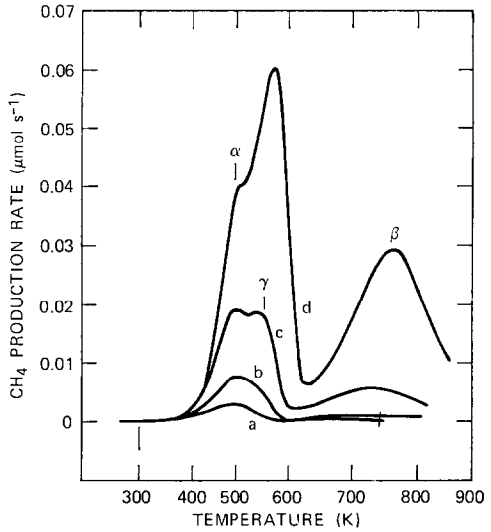

FIG. 3. TPSR of carbon deposited by ethylene decomposition at 575 K. Relative carbon deposit (a) 0.45, (b) 1.4, (c) 3.7, (d) 11.1. Heating rate = 0.9 $K \cdot s^{-1}$.

exposing the catalyst to several CO pulses (0.65 μmol per pulse) injected into a helium stream. The amounts of CO desorbed and CO_2 produced in the effluent stream were measured, from which the amount of carbon deposited could be calculated. Then the catalyst temperature was adjusted to a selected deactivation temperature and maintained for 420 s. After this interval the sample was quickly cooled to 300 K before the carrier gas was switched from helium to hydrogen for TPSR. The TPSR results over the range of deactivation temperatures studied are included in Table 1 and plotted in Arrhenius form in Fig. 4. The α-carbon deactivation rate was presumed to vary in proportion to the amount of α-carbon present. In each experiment, the initial α- to β-carbon ratio was taken as 2.6:1. The results illustrate the increasing rate of configurational transformation of the α species with rising deactivation temperature. Also the β state is thermally unstable, since the area under the curve associated with β-carbon goes

TABLE 1

Thermal Deactivation of Surface Carbon on Ni/Al_2O_3 Catalyst[a]

Catalyst temperature (K)	Deactivation time (s)	Total carbon deposited (μmol)	Carbon configuration after deactivation (μmol)			(C_α) initial / (C_α) final	Effective first-order rate constant k_d (s^{-1})
			C_α	C_β	C_{total}		
557[b]	0	3.6 ± 0.1	2.6	1.0	3.6	—	—
604	480 ± 50	2.8 ± 0.6	1.7	1.3	3.0	1.28	5.1×10^{-4}
668	425 ± 50	2.7 ± 0.4	1.4	1.0	2.4	1.39	7.8×10^{-4}
754	380 ± 80	2.6 ± 0.5	0.8	0.5	1.3	3.35	2.3×10^{-3}
573[c]	0	0.5 ± 0.05	0.47	0.08	0.55	—	—
665[d]	350 ± 50	0.5 ± 0.05	0.20	—	0.20	2.35	2.4×10^{-3}

[a] Surface carbon formed on Ni/Al_2O_3 catalyst (35×10^{-3} g) by exposure to pulses of CO at 557 ± 3 K, except where noted.

[b] Temperature of deposition only; the deposited carbon was immediately cooled to 300 K for subsequent TPSR.

[c] Temperature of carbon deposition from exposure to one C_2H_4 pulse with no deactivation.

[d] Carbon deposition from exposure to a C_2H_4 pulse.

through a maximum as the temperature for deactivation is raised from 557 to 754 K.

Additional data concerning deactivation of α-carbon were obtained from separate isothermal pulse-delay experiments in which the amount of reactive carbon (α state) was determined as a function of "aging" time at a constant deactivation temperature. First, carbon was deposited on the catalyst by exposure to CO pulses in a helium stream at 550 K. The CO pulse was followed by a H_2 pulse after a deactivation period of 10 to 1200 s at a specified temperature. The amount of methane produced by reaction of the hydrogen pulse with the residual reactive α-carbon was determined by gas chromatography. The rate constant for transformation of the reactive carbon was determined from a semilogarithmic plot of methane yield versus deactivation time. These results are included in Fig. 4. The rate constants for the α state transformation exhibit an apparent activation energy of 32 ± 10 kJ mol^{-1} with a first-order frequency factor of 0.4 s^{-1} (calculated by least-squares analysis).

DISCUSSION

The results of our work suggest that the two basic types of surface carbon on alumina-supported nickel are the dispersed (α) and polymerized (β) forms. Evidence for this identification includes the close relationship between the TPSR curves for the α state and the γ bulk carbide state formed by exposure to either CO or C_2H_4, and the observation of greater than monolayer quantities of carbon in both the γ and β states upon repeated exposure to ethylene at 600 K. In TPSR the peak temperatures of both the β and γ states shifted to higher temperatures (Fig. 3) with increasing coverage, as would be expected for a process involving a bulk phase with reaction limited to the surface. Therefore, the α state is considered to represent isolated surface carbon atoms bonded to the nickel, and the β state was taken as amorphous carbon. This identification is consistent with previous studies

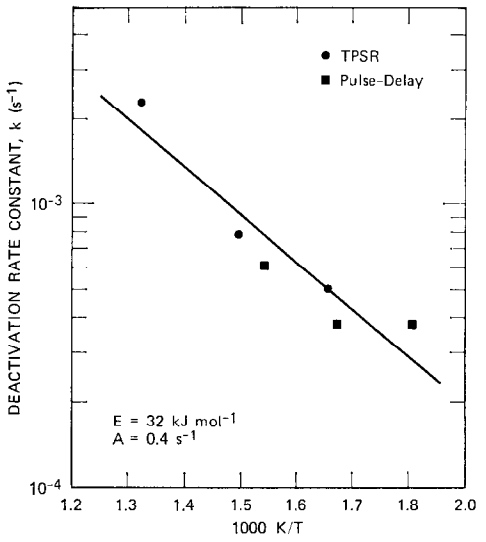

FIG. 4. Deactivation rate constant for transformation of the α-state of surface carbon on Ni/Al_2O_3.

of the nature of carbon chemisorbed on nickel surfaces (*11*, *12*, *14*, *17*, *20*).

Structure and Energetics of Carbon Bound to Nickel Surfaces

The structure and bonding configuration of carbon chemisorbed on well-defined nickel surfaces has been the subject of several recent investigations by low energy electron diffraction (LEED) (*11–14*) and Auger electron spectroscopy (AES) (*11–20*). Two distinct types of surface carbon have been observed on various nickel planes: a dispersed phase that is stable or metastable on Ni(001) and Ni(110) below 600 K, and a hightly polymerized phase that is stable on Ni(111) and Ni(110) at temperatures above 600 K. The dispersed carbon phase on Ni(001) is considered to be made up of single carbon atoms bonded to the nickel lattice at high coordination sites on both flat (*17*) and stepped (*19*) (001) surfaces. On nickel (110), the dispersed form of chemisorbed carbon has been suggested to be composed of diatomic carbon (C_2) species (*21–23*).

The polymerized form of carbon exhibits domains similar to the basal plane of graphite, with little disorder within the domains. The sharpness of the LEED ring patterns suggest the domains probably reach or exceed 15 Å in size on Ni(110) (*11–13*) and Ni(001) (*17*). These domains have preferred orientations on all three index planes.

The energetics of carbon chemisorption on various nickel surfaces have been determined by Blakely *et al.* (*17–19*, *24*) in studies of the equilibrium surface segregation of carbon dissolved in the metal. Based on an endothermic heat of solution of +41.8 kJ mol^{-1} for carbon dissolved in nickel, the heat of formation of carbon chemisorbed in Ni(001) at less than 0.4 monolayer coverage is calculated to be +1.6 kJ mol^{-1}. Therefore, carbon chemisorbed on Ni(001) is just about thermally neutral with respect to graphite. Thus, we expect chemisorbed carbon to be stable on Ni(001) at low coverage (less than 4×10^{14} atoms/cm^2). Segregation of dispersed carbon to the Ni(111) face was not observed (*17*, *19*). Apparently the heat of formation of dispersed chemisorbed carbon on the close-packed nickel face was greater than +42 kJ mol^{-1}. These results show that Ni_3C and carbon chemisorbed on Ni(111), Ni(110), and, at high coverage, on Ni(001) are unstable with respect to elemental carbon, whereas carbon chemisorbed on stepped surfaces and, at low coverage, on Ni(001) is thermodynamically stable. We must note, however, that the effect of chemisorbed CO and O on the thermodynamics of C adsorption is unknown.

Numerous studies of carbon deposition on nickel powders (*25–29*) show two forms of amorphous carbon: a low-density filamentous form and a high-density scale carbon that has some of the properties of crystalline graphite. The filamentous carbon apparently forms at (111) steps and predominantly grows from the (111)

TABLE 2

Methanation Rate Constants[a] for Surface Carbon on Ni/Al_2O_3

Carbon state	Reaction gas	TPSR maximum rate T_p (K)	Energy activation E (kJ mol^{-1})	Preexponential factor log A (s^{-1})	Rate constant k (s^{-1}) at 550 K
α	CO	472 ± 15	71 ± 10	6.46	0.5
β	CO	680 ± 20[b]	130 ± 40	9.2	1.2×10^{-4}
α	C_2H_4	495 ± 10	75	6.46[c]	0.2
γ	C_2H_4	550[b]	84	6.46[c]	0.03
β	C_2H_4	700 ± 20	143	9.2[d]	4×10^{-5}
β	C_3H_8	—	130 ± 12[e]	23.8[e]	2.8×10^{-4}[e]

[a] First-order rate constants for reaction with 10^5 Pa hydrogen. E and A were determined for α(CO) and β(CO) via TPSR heating rate variation.

[b] For $\theta \leq 1$ (based on CO adsorption at 300 K).

[c] The value of A is taken to be equal to that of α(CO).

[d] The value of A is taken to be the same as β(CO).

[e] Zero-order rate from Figueredo and Trimm (*35*); frequency factor has the units molecules cm^{-2} s^{-1} in 100 kPa hydrogen. Rate constant at 550 K is the reciprocal of the time required to gasify 10^{15} carbon atoms cm^{-2}.

faces (*30, 31*). Crystalline graphite platelets are observed on nickel surfaces (*31*) following exposure to carburizing atmospheres at temperatures above 825 K.

Stability of α- and β-Carbon States

Our results demonstrate that α-carbon as a dispersed chemisorbed phase is thermally unstable with respect to β-carbon. Considering the nature of the nickel crystallites (nominal 20 nm in diameter) in the light of the results of Blakely *et al.* (*24*) one might expect dispersed carbon to exhibit a range of binding-energy states and, as a result, a range of transformation rates. Thus on Ni(111) rapid transformation would be favored, but at stepped surfaces sites higher thermal stability would prevail. It is interesting to note that a highly reactive portion of the α state (designated α'-carbon), which appeared as a shoulder at 330 K in TPSR, was more stable than the main α state and may represent carbon chemisorbed at surface dislocations sites, such as steps or kinks.

In addition, the rate of α-carbon transformation appears to be governed by diffusion or nucleation. The low apparent activation barrier for the rate of decrease in α-carbon coverage is suggestive of surface (or bulk) diffusional processes. Levenson *et al.* (*32*) have measured surface diffusion rates of carbon on polycrystalline nickel and report for the variation of the diffusion coefficient (D_s) with temperature: $\log D_s = -4.46 - 1550/T$. For the reported bulk diffusion coefficient of carbon dissolved in nickel (*33*), $\log D_b = -4163 - 4371/T$. One calculates the following values at 625 K: $D_s = 1.1 \times 10^{-7}$ cm^2/s and $D_b = 2.4 \times 10^{-12}$ cm^2/s. Applying these values to carbon surface diffusion on a 20-nm nickel crystallite, one finds a random walk distance after 600 s that is 1300 times greater than the crystallite perimeter. The corresponding random walk distance for bulk diffusion is only 20 times the crystallite diameter. This calculation suggests the transformation is probably not surface-diffusion limited, but controlled by processes involving either bulk diffusion or transformation at the β-carbon–metal interface.

The TPSR results also indicate that filamentous carbon transforms into a more

stable state, possibly free carbon, at a rate no less than an order-of-magnitude slower than the rate of α transformation. It is well known that low-density carbon (*25*, *27*, *34*) is unstable relative to crystalline graphite. Indeed, our results (Table 1) show that some β-carbon is converted at temperatures as low as 668 K into an unreactive, presumably high-density carbon species.

Reactivity of Surface Carbon with Hydrogen

The three carbon states (α, β, γ), characterized by their reactivity toward hydrogen, populate the surface of Ni/Al_2O_3 following exposure to CO at elevated temperatures (Table 2). A measure of the reaction order of α-carbon with respect to H_2 can be obtained from a comparison of our TPSR results with the data obtained under isothermal conditions (*7*). In these experiments carbon was deposited on a nickel film at 523 K by exposure to CO and its reaction rate with H_2 was determined at 64 Pa of H_2 as compared to 100 kPa in our studies. Based on the TPSR results, we calculate at 523 K a methanation rate constant of 0.26 s^{-1} for α-carbon with 100 kPa H_2, as compared to a value (*7*) of 0.0021 s^{-1} at 64 Pa. A more comprehensive study is needed to determine the reaction order with respect to H_2 pressure.

The rates of hydrogenation of the β state measured via TPSR agree well with the rates of hydrogenation of filamentous carbon (*26*, *35*) reported by Figueiredo and Trimm. They studied the reaction with H_2 of carbon deposited on nickel foil and alumina-supported nickel (2.2 m^2/g Ni) by exposure to C_3H_6 in H_2/N_2 mixures at 800 $\pm$ 30 K. The reaction rates were found to follow second-order kinetics with hydrogen pressure and zero-order kinetics with respect to carbon deposited. These data are included in Table 2. The activation energy for carbon gasification was reported (*35*) as 130 $\pm$ 12 kJ/mol. The

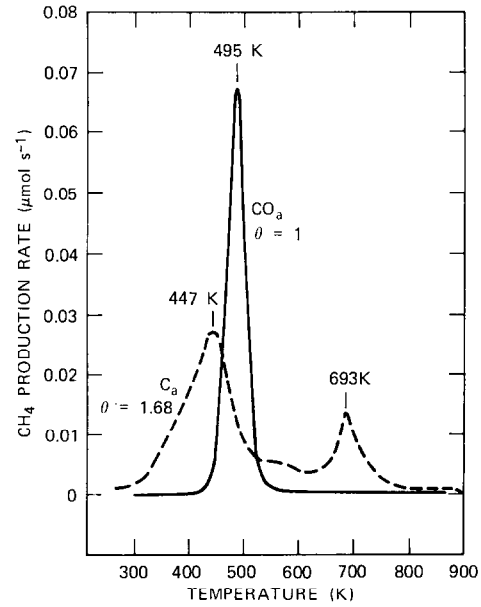

FIG. 5. TPSR of adsorbed CO (300 K) and surface carbon deposited by CO decomposition at 610 K (heating rate = 1.0 K·s^{-1}).

rate at 680 K, 6.5 $\times$ 10^{13} molecules cm^{-2} s^{-1} compares well with the observed TPSR rate, 1.5 $\times$ 10^{13} molecules cm^{-2} s^{-1}, for β-carbon at 680 K. Trimm (*26*, *35*) also demonstrated that the nickel-catalyzed gasification rate was three orders of magnitude greater than the uncatalyzed rate.

In experiments with Ni-impregnated high-surface-area carbon, Tamai *et al.* (*36*, *37*) observed two stages of carbon gasification on exposure to hydrogen at temperatures above 800 K. The reactivity of the carbon depended primarily on the degree of crystallinity of the carbon. Also in the present TPSR study, surface carbon produced by exposure to ethylene and allowed to "age" at 665 K showed CH_4 formation at temperatures >800 K. However we were unable to correlate the loss of α and β carbon with the growth of this nonreactive carbon state because of crystallite sintering and the obscuring production of methane from graphite initially present in the catalyst. Heating a freshly reduced catalyst sample to 900 K in H_2

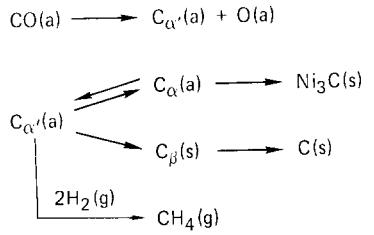

FIG. 6. Interaction of CO with Ni; a = adspecies, s = bulk phase species, g = gaseous species.

produced a large methane peak representing 10 to 20 monolayers and also resulted in some 50 to 80% reduction of surface area measured by CO adsorption. Compared with gasification of β-carbon, gasification of graphite required a temperature higher by about 150 K to reach comparable rates.

The TPSR results for gasification of the initial layers of bulk carbide (Ni_3C) are roughly comparable to rates reported (*38*) for gasification of bulk Ni_3C powder, presuming the surface area was of the order of 5 m^2/g. In that study, initial rates of 4×10^{-9} mol·s^{-1}/mg Ni_3C were reported at 560 K in 66 kPa H_2. However surface areas of the original carbide sample or the reduced samples were not determined.

Mechanism of Synthesis Gas Methanation

Formation of methane and water by dissociative chemisorption of CO and subsequent hydrogenation of the carbon and oxygen adatoms appears to be a plausible mechanism of methanation for the basis of our TPSR results. First of all, on exposing the catalyst to CO at *300 K* and subjecting it to TPSR in H_2 we observed a peak reaction temperature considerably higher than found for α-carbon (Fig. 5). Second, on the basis of our results, we calculate that the α-carbon hydrogenation rates are two orders of magnitude faster than the steady-state methanation rate observed with nickel catalysts (*39*, *40*) for synthesis gas ($H_2/CO = 3/1$). However, this difference may in part be due to inhibition by the high steady-state CO concentration since CO inhibition is observed (*41*) for CO partial pressures above 0.2% in one atmosphere H_2 at 530 ± 15 K.

Apparently CO dissociation, unassisted by formation of an H_xCO surface complex is the rate-determining step. In fact, dissociative chemisorption of CO has been observed at 450 K on Ni(110) and Ni(111) (*42*, *43*) and below 430 K in photoelectrospectroscopy studies on polycrystalline nickel (*5*). Although coadsorbed hydrogen tends to weaken the CO bond (*44*, *45*), infrared spectroscopic studies have not presented any evidence of stable H_xCO structures (*46–48*). Finally, the absence of an H/D kinetic isotope effect has been reported during methanation on supported nickel, which suggests that CO dissociative adsorption is the slow step in the reaction. The available evidence indicates that although CO and H_2 coadsorb on nickel during methanation, the mechanism involves CO dissociation prior to hydrogen addition.

We have summarized our interpretation of the interaction of CO with Ni in Fig. 6. Dissociative adsorption of CO immediately populates a very reactive carbon adatom state (α'), which in the absence of hydrogen forms the α chemisorbed state as a precursor to bulk Ni_3C and β-filament carbon. In the presence of H_2, the α' state is rapidly converted to CH_4. Also the hydrogen produced during C_2H_4 exposure was apparently sufficient to remove this precursor reactive state before significant quantities of β-carbon were formed. Typically, 30% of the carbon deposited after CO exposure at 575 ± 25 K was found to be β-carbon regardless of total coverage, suggesting parallel growth of the α and β forms of surface carbon. In addition, the β state coverage increased only 50% in raising the temperature of CO exposure from 550 to 600 K. These observations suggest that the local surface structure of the nickel crystallite governs the type of

surface carbon formed; that is, one crystal face may produce α-carbon and another may produce β, but the rate of carbon deposition is largely insensitive to structure.

REFERENCES

1. Vannice, M. A., *Catal. Rev.* **14**, 153 (1976).
2. Mills, G. A., and Steffgen, F. W., *Catal. Rev.* **8**, 159 (1973).
3. Fischer, F., and Tropsch, H., *Brennst.-Chem.* **7**, 97 (1926).
4. Kishi, K., and Roberts, W. M., *J. Chem. Soc. Faraday Trans. I* **71**, 1715 (1975).
5. Joyner, R. W., and Roberts, M. W., *J. Chem. Soc. Faraday Trans. I* **70**, 1819 (1974).
6. Wentrcek, P. R., Wood, B. J., and Wise, H., *J. Catal.* **43**, 363 (1976).
7. Araki, M., and Ponec, V., *J. Catal.* **44**, 439 (1976).
8. Craxford, S. F., and Rideal, E. K., *J. Chem. Soc.* 1604 (1939).
9. Smutek, M., Cerny, S., and Buzek, F., *Adv. Catal.* **24**, 343 (1975).
10. Falconer, J. L., and Madix, R. J., *Surf. Sci.* **48**, 393 (1975).
11. Ertl, G., *in* "Molecular Process on Solid Surfaces" (E. Drauglis, R. D. Cretz, and R. I. Jaffee, Eds.), pp. 155–157. McGraw–Hill, New York, 1969.
12. Pitkethly, R. C., *in* "Chemisorption and Catalysis," pp. 107–113. Inst. Petroleum, London, 1970.
13. McCarty, J., and Madix, R. J., *J. Catal.* **38**, 402 (1975).
14. Zuhr, R. A., and Hudson, J. B., *J. Vac. Sci. Tech.* **14**, 431 (1977).
15. Dalmai-Imelik, G., Bertolini, J. C., and Rousseau, J., *Surf. Sci.* **27**, 379 (1971).
16. Blakely, J. M., Kim, J. S., and Potter, H. C., *J. Appl. Phys.* **41**, 2693 (1970).
17. Shelton, J. C., Patil, H. R., and Blakely, J. M., *Surf. Sci.* **43**, 493 (1974).
18. Isett, L. C., and Blakely, J. M., *Surf. Sci.* **47**, 645 (1975).
19. Isett, L. C., and Blakely, J. M., *Surf. Sci.* **58**, 397 (1976).
20. Coad, J. P., and Riviere, J. C., *Surf. Sci.* **25**, 609 (1971).
21. McCarty, J. G., and Madix, R. J., *J. Catal.* **48**, 422 (1977).
22. Zuhr, R. A., and Hudson, J. B., *Surf. Sci.* **66**, 405 (1977).
23. Demuth, J. E., *Chem. Phys. Lett.* **45**, 12 (1977).
24. Isett, L. C., and Blakely, J. M., *J. Vac. Sci. Tech.* **12**, 237 (1975).
25. Rostrup-Nielsen, J. R., *J. Catal.* **27**, 343 (1972).
26. Trimm, D. L., *Inst. Chem. Eng.* **54**, 119 (1976).
27. Renshaw, G. D., Roscoe, C., and Walker, P. L., *J. Catal.* **22**, 394 (1971).
28. Baker, R. T. K., Barber, M. A., Harris, P. S., Feates, F. S., and Waite, R. J., *J. Catal.* **26**, 51 (1972).
29. Baird, J., Fryer, J. B., and Grant, B., *Nature (London)* **233**, 329 (1971).
30. Leidheiser, H., and Gwathmey, A. T., *J. Amer. Chem. Soc.* **70**, 1206 (1948).
31. Grenga, H. E., and Lawless, K. R., *J. Appl. Phys.* **43**, 1508 (1972).
32. Mojica, J. F., and Levenson, L. L., *Surf. Sci.* **59**, 447 (1976).
33. Masaro, T. A., and Petersen, E. E., *J. Appl. Phys.* **42**, 5534 (1971).
34. Dent, J. F., Moignard, L. A., Blackbraun, W. H., and Herbden, D., "An Investigation into the Catalytic Synthesis of Methane by Town Gas Manufacture," 49th Report of the Joint Research Committee of the Gas Research Board and the University of Leeds, GRBZO, 1945.
35. Figueirdo, J. L., and Trimm, D. L., *J. Catal.* **40**, 154 (1975).
36. Tomita, A., Sato, N., and Tamai, Y., *Carbon* **12**, 143 (1974).
37. Tomita, A., and Tamai, Y., *J. Catal.* **27**, 293 (1972).
38. Galway, A. K., *J. Catal.* **1**, 227 (1962).
39. Vannice, M. A., *J. Catal.* **37**, 462 (1975).
40. Dalla Betta, R. A., Piken, A. G., and Shelef, M., *J. Catal.* **40**, 173 (1975).
41. Schoubye, P., *J. Catal.* **14**, 238 (1969).
42. Madden, H. H., and Ertl, G., *Surf. Sci.* **35**, 211 (1973).
43. Christmann, K., Schober, O., and Ertl, G., *J. Chem. Phys.* **60**, 4719 (1974).
44. Conrad, H., Ertl, G., Kuppers, J., and Latke, E. E., *in* "Proceedings of the Sixth International Catalysis Conference," Vol. 1, p. 426. London, 1976.
45. Primet, M., and Sheppard, N., *J. Catal.* **41**, 258 (1976).
46. Eischens, R. P., and Pliskin, W. A., *Adv. Catal.* **10**, 1 (1958).
47. Blyholder, G., and Neff, L. D., *J. Catal.* **2**, 138 (1963).
48. Martin, G. A., Dalmon, J. A., and Primet, M., *C.R. Acad. Sci. Paris* **284C**, 163 (1977).
49. Dalla Betta, R. A., and Shelef, M., *J. Catal.* **49**, 383 (1977).